ICASSP 2023 - 2023 IEEE International Conference on Acoustics, Speech and Signal Processing (ICASSP) | 978-1-7281-6327-7/23/$31.00 ©2023 IEEE | DOI: 10.1109/ICASSP49357.2023.10095315

# SUBSPACE-BASED DETECTOR FOR DISTRIBUTED MMWAVE MIMO RADAR SENSORS

*Moein Ahmadi, Mohammad Alaee-Kerahroodi, Bhavani Shankar M. R., and Björn Ottersten*

Interdisciplinary Centre for Security, Reliability and Trust (SnT), University of Luxembourg

## ABSTRACT

Driven by emerging applications, mmWave radars are increasingly being integrated into indoor scene monitoring systems due to their ability to provide high accuracy range, velocity, and angle information of the objects. This paper addresses the problem of moving target detection in a connected, distributed Multiple-Input Multiple-Output (MIMO) radar sensor network designed as an indoor scene monitoring system. We propose a general signal model for distributed connected MIMO radar sensors that collect unwanted and interference signals in a low-rank subspace based on their angle and Doppler frequency spread with different subspace coefficients. We use Generalized Likelihood Ratio Test (GLRT) for moving target detection and find the best detector while demonstrating that it has a constant false alarm rate. The performance of the proposed detector is validated by Monte-Carlo simulation.

***Index Terms***— Adaptive detection, clutter subspace, distributed MIMO radar, GLRT, indoor sensing.

## 1. INTRODUCTION

Recently, there has been a lot of interest in Multiple-Input Multiple-Output (MIMO) radar having multiple transmit/receive antennas for both civilian and military purposes. There are two main categories: distributed MIMO radar, where the antennas are widely separated from each other, and colocated MIMO radar, where the antennas in the TX and, correspondingly, RX array are closely spaced [1]. The distributed radar configuration allowing the radar to exploit the spatial and geometric diversity to enhance target detection performance. Waveform diversity can be exploited in colocated MIMO radar to improve spatial resolution [2]. Some benefits of this kind of radar include large virtual array length, improved parameter identifiability, improved interference suppression, and more adaptable beampattern design.

The received signal in any radar system is typically composed of target data, receiver noise, clutter echo, and other sources of interference. The detection task in a network-based radar system, like the single sensor, examines the echo data to determine whether or not a target of interest is present. To that end, several detectors have been proposed in the literature, to name a few, see [3], [4], [5], [6], [7]. In, [8] moving target detection with a distributed MIMO radar in spatially nonhomogeneous clutter environments is considered, where every radar station is modeled as a single antenna transceiver and the interference model is in Doppler frequency domain. Authors in [9] consider the problem of moving target detection in phased-MIMO radar on an airborne platform. However, none of the aforementioned studies are considering detector design for distributed sensors in indoor scene monitoring applications. In this scenario, usually Frequency Modulated Continuous Wave (FMCW) Millimeter-Wave (mmWave) radars are used. In this context in [10], a low complexity detector is presented for indoor scenario, but the sensor is a single monostatic radar. Researchers in [11] study a 3D-Constant False Alarm Rate (CFAR) algorithm to detect drones with a colocated MIMO radar, not a network-based radar system. In [12], a two-level CFAR detector for mmWave radar is proposed; however, this does not consider the interference subspace. to the interference subspace. In [13], a CFAR detector was derived for a single radar with general antenna array configuration consisting of primary channels with high-gain beams and reference channels with low-gain beams. Thus the performance of a detection scheme in network MIMO radar is still open.

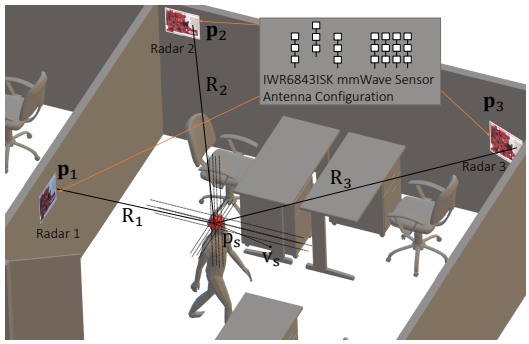


**Fig. 1**: Distributed MIMO radar sensors configuration.

Unlike the previous studies, we analytically design an optimal detector for a network of MIMO radar sensors for indoor scene monitoring application, to detect moving targets which are embedded in clutter, interference, and noise, as illustrated graphically in Figure 1. We present a signal model for the considered case, which contains both signal dependent

This work was supported by FNR BRIDGES MASTERS under grant BRIDGES2020/IS/15407066/MASTERS.

and independent interferences with varying coefficient values based on the geometry and reflectivity of each interference. Based on the developed signal model, we construct a Generalized Likelihood Ratio Test (GLRT) detector and derive its statistical properties in closed form for both the null and alternative hypotheses. Furthermore, we demonstrate analytically that the proposed GLRT is a CFAR detector. We show that the proposed subspace detector outperforms classical detectors when the clutter to noise ratio on the subspace of interest exceeds the orthogonal subspace matrix loss. In the case of a distributed target model with fluctuating Radar Cross Section (RCS), the proposed detector can take advantage of spatial and geometric diversity to improve target detection performance because radar sensors in a network can probe the scene from different aspect angles. In this case, even with the same post processing Signal to Interference and Noise Ratio (SINR), the distributed radar configuration outperforms a single colocated MIMO radar.

The remainder of this paper is organized as follows[1]. Section 2 introduces the signal model and problem formulation for distributed MIMO radar network. In addition, the signature matrix of interference for distributed MIMO radar is derived. In Section 3, the GLRT detector is derived. Section 4 contains the simulation results. Finally, conclusions are drawn in Section 5.

## 2. SIGNAL MODEL AND PROBLEM FORMULATION

We consider a distributed radar system with $Q$ colocated mmWave MIMO radar sensors, each have $M_q$ transmit antenna elements, and $N_q$ receive antenna elements. Assume that $\mathbf{p}_q = [x_q, y_q, z_q]^T$ denotes the absolute position of the $q$th radar sensor, where $x_q$, $y_q$, and $z_q$ represents the absolute Cartesian coordinates, with $q = 1, 2, \ldots, Q$. In this case, a target with absolute position $\mathbf{p}_s = [x_s, y_s, z_s]^T$ and absolute velocity $\mathbf{v}_s = [v_{xs}, v_{ys}, v_{zs}]^T$, will have a relative distance $R_q$, azimuth $\theta_q$, and elevation $\phi_q$ with the $q$th radar sensor as indicated in Figure 1.

The target received signal from $L_q$ chirps (pulses) in one Coherent Processing Interval (CPI) can be expressed as,

$$\mathbf{x}_q = \alpha_q \mathbf{s}_q(\theta_q, \phi_q, f_{d,q}) + \mathbf{c}_q + \mathbf{n}_q \in \mathbb{C}^{L_q M_q N_q} \quad (1)$$

where $\alpha_q = \sqrt{\beta_q \frac{P_t G_t G_r \lambda^2 \sigma_q}{(4\pi)^3 R_q^4 L_{sp}}}$ indicates the amplitude of the reflected signal at the $q$th radar sensors, $\lambda$ is the wavelength, $P_t$ is the transmit power, $G_t$ and $G_r$ are the transmit and receive antenna gains. Further, $\sigma_q$ is the RCS at $q$th radar sensor, which has diversity due to the different look angles from every sensor to a target. Finally, $L_{sp}$ is the summation of consolidates the system and propagation losses, and $\beta_q$ is the receiver input impedance. In (1), $\mathbf{c}_q$ and $\mathbf{n}_q$ denote clutter and noise respectively. We assume, $\mathbf{n}_q \sim \mathcal{CN}(\mathbf{0}, \sigma^2\mathbf{I})$ is the thermal noise in the receiver and it which has a white noise Power Spectral Density (PSD) with $P(f) = k_B T_0$, where $k_B$ is the Boltzmann constant and $T_0$ is the effective noise temperature. The receiver acts as a filter with bandwidth $B$ to shape the white noise PSD, then the total noise power at the output of the receiver is $k_B T_0 B F_n$ where $F_n$ is the receiver noise factor. Further, the signal steering vector is, $\mathbf{s}_q(\theta_q, \phi_q, f_{d,q}) = \mathbf{a}_q(\theta_q, \phi_q) \otimes \mathbf{b}_q(\theta_q, \phi_q) \otimes \mathbf{d}_q(f_{d,q})$, where $\mathbf{a}_q(\theta, \phi) = [e^{-j\mathbf{k}^T(\theta,\phi)\mathbf{p}^{tx}_{q,1}}, \ldots, e^{-j\mathbf{k}^T(\theta,\phi)\mathbf{p}^{tx}_{q,M_q}}]^T$, and $\mathbf{b}_q(\theta, \phi) = [e^{-j\mathbf{k}^T(\theta,\phi)\mathbf{p}^{rx}_{q,1}}, \ldots, e^{-j\mathbf{k}^T(\theta,\phi)\mathbf{p}^{rx}_{q,N_q}}]^T$, are the spatial transmit and receive steering vectors, respectively, and $\mathbf{k}(\theta, \phi) = \frac{2\pi}{\lambda}[\cos\theta\cos\phi, \sin\theta\cos\phi, \sin\phi]^T$ is the wavenumber vector with $\theta$ and $\phi$ are azimuth and elevation angles, respectively. $\mathbf{p}^{tx}_{q,m}$ and $\mathbf{p}^{rx}_{q,n}$ are the locations of the $q$th radar transmit and receive array elements. Further, $\mathbf{d}_q(f_{d,q}) = [1, e^{j2\pi f_{d,q} T_p}, ..., e^{j2\pi f_{d,q}(L_q-1)T_p)}]^T$, where $T_p$ is the chirp (pulse) repetition interval and $f_{d,q}$ is the Doppler frequency of the target relative to $q$th radar sensor, specified as, $f_{d,q} = \frac{2\mathbf{v}_s^T(\mathbf{p}_s - \mathbf{p}_q)}{\lambda \|\mathbf{p}_s - \mathbf{p}_q\|}$.

At the fusion center, the received signals can be stacked by $\mathbf{x} = [\mathbf{x}_1^T, \mathbf{x}_2^T, ..., \mathbf{x}_Q^T]^T$, $\mathbf{c} = [\mathbf{c}_1^T, \mathbf{c}_2^T, ..., \mathbf{c}_Q^T]^T$, $\mathbf{n} = [\mathbf{n}_1^T, \mathbf{n}_2^T, ..., \mathbf{n}_Q^T]^T$, and $\boldsymbol{\alpha} = [\alpha_1, \alpha_2, ..., \alpha_Q]^T$. By defining steering matrix $\mathbf{S} \in \mathbb{C}^{\sum_{q=1}^{Q} M_q N_q L_q \times Q}$ as,

$$\mathbf{S} = \begin{bmatrix} \mathbf{s}_1(\theta_1, \phi_1, f_{d,1}) & \mathbf{0}_{L_1 M_1 N_1 \times 1} & \cdots & \mathbf{0}_{L_1 M_1 N_1 \times 1} \\ \mathbf{0}_{L_2 M_2 N_2 \times 1} & \mathbf{s}_2(\theta_2, \phi_2, f_{d,2}) & \cdots & \mathbf{0}_{L_2 M_2 N_2 \times 1} \\ \vdots & \vdots & \ddots & \vdots \\ \mathbf{0}_{L_Q M_Q N_Q \times 1} & \mathbf{0}_{L_Q M_Q N_Q \times 1} & \cdots & \mathbf{s}_Q(\theta_Q, \phi_Q, f_{d,Q}) \end{bmatrix}$$

The fused received signal then can be obtained by[2], $\mathbf{x} = \mathbf{S}\boldsymbol{\alpha} + \mathbf{c} + \mathbf{n}$. Let $\mathbf{c}_q = \mathbf{A}_q \mathbf{g}_q$, where $\mathbf{A}_q \in \mathbb{C}^{M_q N_q L_q \times H_q}$ defines the interference subspace with $H_q$ as the interference matrix rank. The interference signals in this case, depend on Doppler spectrum spread and also spatial locations of high RCS stationary scatterers. Assume that the region of interfering scatterers is $\theta^{int}_{q,1} < \theta_q < \theta^{int}_{q,2}$ in azimuth, $\phi^{int}_{q,1} < \phi_q < \phi^{int}_{q,2}$ in elevation, and $f^{int}_{d,q,1} < f_{d,q} < f^{int}_{d,q,2}$ in Doppler frequency. Then, $\mathbf{A}_q = [\mathbf{s}_q(\theta_{q,1}, \phi_{q,1}, f_{d,q,1}), \ldots, \mathbf{s}_q(\theta_{q,H_q}, \phi_{q,H_q}, f_{d,q,H_q})]$. Further, $\mathbf{g}_q \in \mathbb{C}^{H_q}$ is an unknown deterministic complex vector coefficients related to each column of $\mathbf{A}_q$ matrix. By defining of $\mathbf{g} = [\mathbf{g}_1^T, \mathbf{g}_2^T, ..., \mathbf{g}_Q^T]^T$, and

$$\mathbf{A} = \begin{bmatrix} \mathbf{A}_1 & \mathbf{0}_{L_1 M_1 N_1 \times H_2} & \ldots & \mathbf{0}_{L_1 M_1 N_1 \times H_Q} \\ \mathbf{0}_{L_2 M_2 N_2 \times H_1} & \mathbf{A}_2 & \ldots & \mathbf{0}_{L_2 M_2 N_2 \times H_Q} \\ \vdots & \vdots & \ddots & \vdots \\ \mathbf{0}_{L_Q M_Q N_Q \times H_1} & \mathbf{0}_{L_Q M_Q N_Q \times H_2} & \ldots & \mathbf{A}_Q \end{bmatrix}$$

[1]Notations: The matrices and vectors are denoted by uppercase and lowercase bold letters, respectively. $(.)^T$ and $(.)^H$ stand for the transpose and Hermitian transpose, respectively. Identity matrix, Kronecker product product are respectively represented by $\mathbf{I}$, $\otimes$. Also, $\|.\|$ denotes the Euclidean norm of a vector.

[2]Different sources of interference can be present in indoor scene monitoring using multiple sensors. First, because high RCS objects are present in the scene, a reflected signal from these objects can be regarded as parallel-slope interference. Second, multiple radars are available in the scene which may result in a similar-slope or sweeping-slope interference [14].

$\mathbf{A} \in \mathbb{C}^{\sum_{q=1}^{Q} M_q N_q L_q \times \sum_{q=1}^{Q} H_q}$. the interference signal can be expressed as $\mathbf{c} = \mathbf{A}\mathbf{g}$. Let $\mathcal{H}_0$ represent the null hypothesis that the target is absent, and $\mathcal{H}_1$ represent the alternative hypothesis that the target is present. The detection problem can be cast as the following binary hypothesis test

$$\begin{cases} \mathcal{H}_0: & \mathbf{x} = \mathbf{A}\mathbf{g} + \mathbf{n} \\ \mathcal{H}_1: & \mathbf{x} = \mathbf{S}\boldsymbol{\alpha} + \mathbf{A}\mathbf{g} + \mathbf{n} \end{cases} \tag{2}$$

In the sequel, we propose an optimum detector based on GLRT.

## 3. GLRT-BASED DETECTOR DESIGN

The GLRT detector is obtained by,

$$t_{\text{GLRT}} = \ln \frac{\max\limits_{\mathbf{g},\boldsymbol{\alpha}} p(\mathbf{x}|\mathcal{H}_1)}{\max\limits_{\mathbf{g}} p(\mathbf{x}|\mathcal{H}_0)} \underset{\mathcal{H}_0}{\overset{\mathcal{H}_1}{\gtrless}} \eta \tag{3}$$

where $p(\mathbf{x}|\mathcal{H}_0)$ and $p(\mathbf{x}|\mathcal{H}_1)$ are the Probability Density Function (PDF) of $\mathbf{x}$ under $\mathcal{H}_0$ and $\mathcal{H}_1$, respectively. Mathematically, $p(\mathbf{x}|\mathcal{H}_0) = \frac{1}{(\pi\sigma^2)^{\Omega}} \exp(-\frac{(\mathbf{x}-\mathbf{A}\mathbf{g})^H(\mathbf{x}-\mathbf{A}\mathbf{g})}{\sigma^2})$, where $\Omega = \sum_{q=1}^{Q} L_q M_q N_q$ and $\sigma^2$ is the variance of additive white Gaussian noise and $p(\mathbf{x}|\mathcal{H}_1) = p(\mathbf{x} - \mathbf{S}\boldsymbol{\alpha}|\mathcal{H}_0)$. Under alternative hypothesis, $\mathcal{H}_1$, the Maximum Likelihood (ML) estimations for $\mathbf{g}$ and $\boldsymbol{\alpha}$ can be obtained by solving

$$\min_{\mathbf{g},\boldsymbol{\alpha}} (\mathbf{x} - \mathbf{S}\boldsymbol{\alpha} - \mathbf{A}\mathbf{g})^H (\mathbf{x} - \mathbf{S}\boldsymbol{\alpha} - \mathbf{A}\mathbf{g}). \tag{4}$$

The maximum likelihood estimation of the interference coefficient vector under $\mathcal{H}_1$ is given by

$$\hat{\mathbf{g}}_1 = (\mathbf{A}^H\mathbf{A})^{-1}\mathbf{A}^H(\mathbf{x} - \mathbf{S}\boldsymbol{\alpha}) \tag{5}$$

with substituting (5) in (4), the ML estimation of $\boldsymbol{\alpha}$ is obtained by

$$\min_{\boldsymbol{\alpha}} (\mathbf{x} - \mathbf{S}\boldsymbol{\alpha})^H (\mathbf{I} - \mathbf{A}(\mathbf{A}^H\mathbf{A})^{-1}\mathbf{A}^H)(\mathbf{x} - \mathbf{S}\boldsymbol{\alpha}), \tag{6}$$

then the maximum likelihood estimation of $\boldsymbol{\alpha}$ under $\mathcal{H}_1$ is given by

$$\hat{\boldsymbol{\alpha}} = (\mathbf{S}^H\mathbf{P}_{\mathbf{A}}\mathbf{S})^{-1}\mathbf{S}^H\mathbf{P}_{\mathbf{A}}^{\perp}\mathbf{x} \tag{7}$$

where $\mathbf{P}_{\mathbf{A}}^{\perp} = \mathbf{I} - \mathbf{A}(\mathbf{A}^H\mathbf{A})^{-1}\mathbf{A}^H$, is the orthogonal projection on the subspace spanned by $\mathbf{A}$. By setting $\boldsymbol{\alpha} = \mathbf{0}$ in (5), the ML estimation of $\boldsymbol{\alpha}$ under $\mathcal{H}_0$ is,

$$\hat{\mathbf{g}}_0 = (\mathbf{A}^H\mathbf{A})^{-1}\mathbf{A}^H\mathbf{x} \tag{8}$$

Substituting (5),(7) and (8) in (3) lead to

$$t_{\text{GLRT}} = \frac{1}{\sigma^2}\mathbf{x}^H\mathbf{P}_{\mathbf{A}}^{\perp}\mathbf{S}(\mathbf{S}^H\mathbf{P}_{\mathbf{A}}^{\perp}\mathbf{S})^{-1}\mathbf{S}^H\mathbf{P}_{\mathbf{A}}^{\perp}\mathbf{x} \underset{\mathrm{H}_0}{\overset{\mathrm{H}_1}{\gtrless}} \eta \tag{9}$$

Since the noise, $\mathbf{n}$, has complex Gaussian distribution with zero mean and covariance matrix $\sigma^2\mathbf{I}$, i.e., $\mathbf{n} \sim \mathcal{CN}(\mathbf{0}, \sigma^2\mathbf{I})$, $\mathbf{P}_{\mathbf{A}}^{\perp}\mathbf{A} = \mathbf{0}$, and also because $\mathbf{S}^H\mathbf{P}_{\mathbf{A}}^{\perp}\mathbf{S}$ is a full-rank matrix, then $\text{rank}(\mathbf{P}_{\mathbf{A}}^{\perp}\mathbf{S}(\mathbf{S}^H\mathbf{P}_{\mathbf{A}}^{\perp}\mathbf{S})^{-1}\mathbf{S}^H\mathbf{P}_{\mathbf{A}}^{\perp}) = Q$, and the statistical distributions of the GLRT test variable (9) under both the null and alternative hypotheses are $t_{\text{GLRT},\mathcal{H}_0} \sim \chi^2_{2Q}(0)$ and $t_{\text{GLRT},\mathcal{H}_1} \sim \chi^2_{2Q}(\frac{1}{\sigma^2}\boldsymbol{\alpha}^H\mathbf{S}^H\mathbf{P}_{\mathbf{A}}^{\perp}\mathbf{S}\boldsymbol{\alpha})$ , where $\chi^2_N(\gamma)$ denotes a noncentral chi-square distribution with $N$ degrees of freedom and noncentrality parameter $\gamma$. Consequently, the probability of false alarm of GLRT detector is given by $P_{fa} = \Pr(t_{\text{GLRT}} > \eta|\mathcal{H}_0) = e^{-\eta}\sum_{q=0}^{Q-1}\frac{\eta^q}{q!}$. Note that the probability of false alarm is independent of the nuisance parameters, i.e., $\mathbf{g}$ and the noise variance $\sigma^2$, and hence, the proposed detector is a constant false alarm rate detector. The probability of detection of GLRT detector is given by $P_d = \Pr(t_{\text{GLRT}} > \eta|\mathcal{H}_1) = \mathcal{M}_Q\left(\sqrt{\frac{2}{\sigma^2}\boldsymbol{\alpha}^H\mathbf{S}^H\mathbf{P}_{\mathbf{A}}^{\perp}\mathbf{S}\boldsymbol{\alpha}}, \sqrt{2\eta}\right)$, where $\mathcal{M}_K(a,b) = \exp(-\frac{a^2+b^2}{2})\sum_{k=1-K}^{\infty}(\frac{a}{b})^k I_k(ab)$, is the Marcum Q-function and $I_k(.)$ is the modified Bessel function of the first kind of order $k$. Defining the post processing signal to interference pulse noise ratio as $\text{SINR}_{\text{Post}} = \frac{1}{\sigma^2}\boldsymbol{\alpha}^H\mathbf{S}^H\mathbf{P}_{\mathbf{A}}^{\perp}\mathbf{S}\boldsymbol{\alpha}$ results in $P_d = \mathcal{M}_Q(\sqrt{2\text{SINR}_{\text{Post}}}, \sqrt{2\eta})$.

The GLRT detector requires noise variance; this can be estimated from secondary data $\mathbf{x}_i \sim \mathcal{CN}(\mathbf{A}\mathbf{g}, \sigma^2\mathbf{I})$; $i = 1, 2, \ldots, K$, where $K$ is the number of secondary data from adjacent range gates where $p(\mathbf{x}_1, \mathbf{x}_2, \ldots, \mathbf{x}_K) = \frac{1}{(\pi\sigma^2)^{K\Omega}}\exp(-\frac{1}{\sigma^2}\sum_{q=1}^{Q}(\mathbf{x}_q - \mathbf{A}_q\mathbf{g}_q)^H(\mathbf{x}_q - \mathbf{A}_q\mathbf{g}_q))$. Using [9], $\arg\max_{\mathbf{A}} |\mathbf{A}|^{-L}\exp(-\text{Tr}(\mathbf{A}^{-1}\mathbf{B})) = \frac{1}{L}\mathbf{B}$, the ML estimation of $\sigma^2$ can be obtained as $\hat{\sigma}^2 = \frac{1}{KT}\sum_{q=1}^{Q}(\mathbf{x}_q - \mathbf{A}_q\mathbf{g}_q)^H(\mathbf{x}_q - \mathbf{A}_q\mathbf{g}_q)$. By using the ML estimation $\hat{\mathbf{g}}_q = (\mathbf{A}_q^H\mathbf{A}_q)^{-1}\mathbf{A}_q^H\mathbf{x}_q$, then $\hat{\sigma}^2 = \frac{1}{K\Omega}\sum_{q=1}^{Q}\mathbf{x}_q\mathbf{P}_{\mathbf{A}_q}^{\perp}\mathbf{x}_q$ ,where $\mathbf{P}_{\mathbf{A}_q}^{\perp}$ is the orthogonal projection on the subspace spanned by $\mathbf{A}_q$. Therefore, the adaptive GLRT detector can be obtained by

$$t_{\text{AD}} = \frac{K\Omega}{\sum_{q=1}^{Q}\mathbf{x}_q\mathbf{P}_{\mathbf{A}_q}^{\perp}\mathbf{x}_q}\mathbf{x}^H\mathbf{P}_{\mathbf{A}}^{\perp}\mathbf{S}(\mathbf{S}^H\mathbf{P}_{\mathbf{A}}^{\perp}\mathbf{S})^{-1}\mathbf{S}^H\mathbf{P}_{\mathbf{A}}^{\perp}\mathbf{x} \underset{\mathrm{H}_0}{\overset{\mathrm{H}_1}{\gtrless}} \eta \tag{10}$$

The estimation of $\hat{\sigma}^2$ has the chi-square distribution with $2K\Omega - 2r$ degree of freedom, where $r = \text{rank}(\mathbf{A}_q)$. Therefore, the adaptive detector of (10) has the F-distribution [15] with $2Q$ and $2K\Omega - 2r$ degrees of freedom. Hence, we obtain $\mathrm{P}_{\mathrm{fa-AD}} = \widetilde{I}_{\frac{\eta\Omega}{\eta\Omega+\mathrm{K}\Omega-r}}(\mathrm{Q}, \mathrm{K}\Omega - r)$, where $\widetilde{I}_k(.,.)$ is the regularized incomplete beta function. As seen, the probability of false alarm is independent of the statistical property of the noise and has a constant false alarm rate property.

## 4. SIMULATION AND RESULTS

In this section, numerical examples are provided to assess the performance of the proposed detector. By considering multiple of TI IWR6843ISK sensors [16], in the sequel we analyze the detection performance and demonstrate the benefits of the connected MIMO radar sensors for indoor scene monitoring

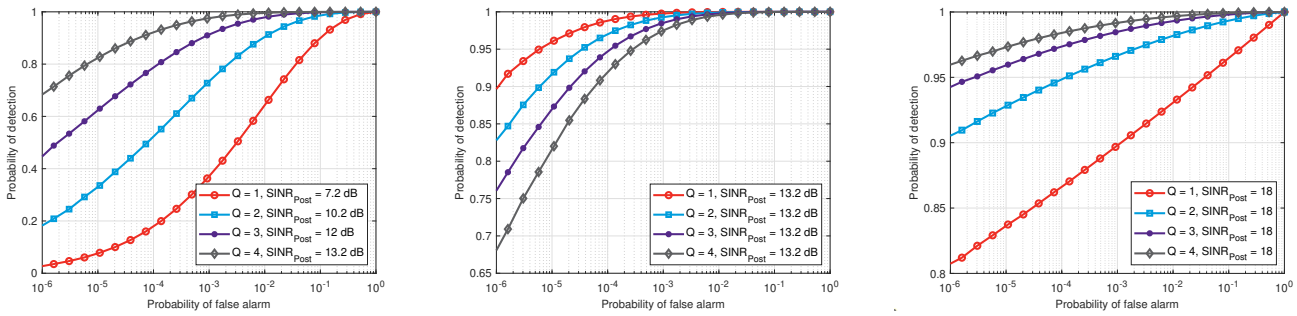


(a) (b) (c)

**Fig. 2**: Receiver Operating Characteristic (ROC) curves for proposed detector and $Q = 1, 2, 3, 4$ distributed sensors a) targets with identical and non-fluctuating RCS, b) same $\text{SINR}_{\text{Post}}$ and nonfluctuant RCS, and c) same $\text{SINR}_{\text{Post}}$ and fluctuant RCS.

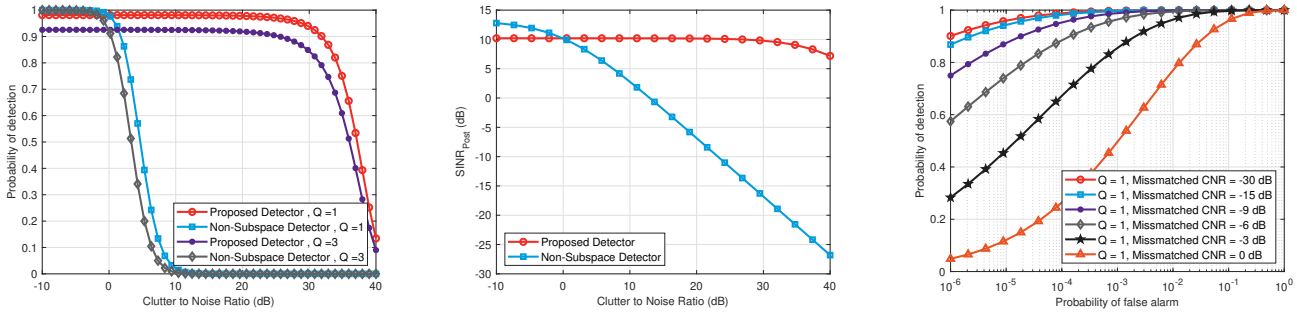


(a) (b) (c)

**Fig. 3**: a) $\text{P}_\text{d}$ vs. CNR for the proposed GLRT detector, $\text{P}_\text{fa} = 10^{-6}$ and $\text{SNR}_{\text{Post}}$=17 dB. b) $\text{SINR}_{\text{Post}}$ vs. CNR, $\text{SNR}_{\text{Post}}$=13.2 dB. c) Interference subspace matrix mismatch effect on ROC curves for the proposed GLRT Detector.

applications. In Figure 2, detection performance in terms of the ROC is evaluated for different number of mmWave MIMO radars. In Figure 2a, we consider targets with same RCS for different sensor number, and thus increasing the number of sensors provides better post processing SINR and, as a result, better performance. In Figure 2b, we consider the case where the post-processing SINR is similar for all the configurations, despite the increased number of sensors. In this scenario, target RCS is adjusted such that SINR in the distributed and colocated case be the same. In this case, since both distributed and colocated systems receive similar SINR from target, then coherent integration in the colocated obtains better performance. Figure 2c shows that when we have fluctuant target amplitude, due to RCS diversity gain, increasing the number of sensors improves detection performance even with the same post processing SINR.

Figure 3a depicts the detection performance of the proposed subspace-based detector. When the interference signal is much stronger than the noise, the proposed subspace performs better in terms of detection. For high clutter to noise values, as shown in Figure 3b, the proposed detector can suppress interference and achieve higher post processing SINR, resulting in better detection performance. Figure 3c shows the effect of interference subspace matrix mismatch on the proposed detector. When perfect information of the actual interference subspace is available, the proposed detector can suppress the interference component. If the mismatch matrix part is $\tilde{\mathbf{A}}$ , then the detector output is a noncentral chi-square distribution with $2Q$ degrees of freedom and noncentrality parameter $\frac{1}{\sigma^2}\mathbf{g}^H\tilde{\mathbf{A}}^H\mathbf{P}_{\mathbf{A}}^{\perp}\tilde{\mathbf{A}}\mathbf{g}$ and $\frac{1}{\sigma^2}(\boldsymbol{\alpha}^H\mathbf{S}^H\mathbf{P}_{\mathbf{A}}^{\perp}\mathbf{S}\boldsymbol{\alpha} + \mathbf{g}^H\tilde{\mathbf{A}}^H\mathbf{P}_{\mathbf{A}}^{\perp}\tilde{\mathbf{A}}\mathbf{g})$ under $\mathcal{H}_0$ and $\mathcal{H}_1$ respectively.

## 5. CONCLUSION

The paper devises a GLRT based detector for distributed radar exploiting lower dimensional clutter subspace, determines its performance analytically and offers insights into system operation. When identical post-processing SINR is considered for each sensor, single colocated MIMO outperforms distributed counterparts in non fluctuating RCS target detection. In a more realistic scenario with a constant RCS target, the distributed radar configuration outperforms the single sensor case. Distributed radars can see the target from various aspect angles and exploit RCS diversity in the case of fluctuating RCS targets. In this case, the distributed radar configuration outperforms the single colocated MIMO radar even with the same post-processing SINR. Finally, when the clutter to noise ratio exceeds the orthogonal subspace matrix loss on the subspace of signal of interest, the proposed subspace detector outperforms the classical detector.

## 6. REFERENCES


[1] Shunqiao Sun, Athina P. Petropulu, and H. Vincent Poor, "MIMO radar for advanced driver-assistance systems and autonomous driving: Advantages and challenges," *IEEE Signal Processing Magazine*, vol. 37, no. 4, pp. 98–117, 2020.

[2] Victor Chernyak, "Multisite radar systems composed of MIMO radars," *IEEE Aerospace and Electronic Systems Magazine*, vol. 29, no. 12, pp. 28–37, 2014.

[3] Shabnam Ghotbi, Moein Ahmadi, and Mohammad Ali Sebt, "Moving target detection in airborne MIMO radar for fluctuating target RCS model," in *2014 22nd European Signal Processing Conference (EUSIPCO)*, 2014, pp. 1701–1705.

[4] Jun Liu and Jian Li, "Robust detection in MIMO radar with steering vector mismatches," *IEEE Transactions on Signal Processing*, vol. 67, no. 20, pp. 5270–5280, 2019.

[5] Hongbin Li, Fangzhou Wang, Cengcang Zeng, and Mark A. Govoni, "Signal detection in distributed MIMO radar with non-orthogonal waveforms and sync errors," *IEEE Transactions on Signal Processing*, vol. 69, pp. 3671–3684, 2021.

[6] Xiangyu Gao, Guanbin Xing, Sumit Roy, and Hui Liu, "Experiments with mmwave automotive radar test-bed," in *2019 53rd Asilomar Conference on Signals, Systems, and Computers*, 2019, pp. 1–6.

[7] M.A. Richards, *Fundamentals Of Radar Signal Processing*, McGraw-Hill Education (India) Pvt Limited, 2005.

[8] Pu Wang, Hongbin Li, and Braham Himed, "Moving target detection using distributed MIMO radar in clutter with nonhomogeneous power," *IEEE Transactions on Signal Processing*, vol. 59, no. 10, pp. 4809–4820, 2011.

[9] Shabnam Ghotbi, Moein Ahmadi, and Kamal Mohamedpour, "Moving target detection under spatially non-homogeneous clutter for airborne phased-MIMO radar," in *2015 IEEE Radar Conference*, 2015, pp. 82–86.

[10] Ali Safa, Tim Verbelen, Lars Keuninckx, Ilja Ocket, Mathias Hartmann, André Bourdoux, Francky Catthoor, and Georges G. E. Gielen, "A low-complexity radar detector outperforming os-cfar for indoor drone obstacle avoidance," *IEEE Journal of Selected Topics in Applied Earth Observations and Remote Sensing*, vol. 14, pp. 9162–9175, 2021.

[11] Siying Wang and Reinhold Herschel, "Fast 3D-CFAR for drone detection with MIMO radars," in *2021 18th European Radar Conference (EuRAD)*, 2022, pp. 209–212.

[12] Chuanwen Xu, Fenggui Wang, Yanbo Zhang, Li Xu, Mingshun Ai, and Guang Yan, "Two-level CFAR algorithm for target detection in mmWave radar," in *2021 International Conference on Computer Engineering and Application (ICCEA)*, 2021, pp. 240–243.

[13] Jun Liu, Dian Jin, Weijian Liu, Danilo Orlando, and Alfonso Farina, "Polarimetric GLRT for adaptive detection in general array configuration," *IEEE Transactions on Signal Processing*, vol. 70, pp. 4201–4211, 2022.

[14] Robin Amar, Mohammad Alaee-Kerahroodi, and M. R. Bhavani Shankar, "FMCW-FMCW interference analysis in mm-wave radars; an indoor case study and validation by measurements," in *2021 21st International Radar Symposium (IRS)*, 2021, pp. 1–11.

[15] M. Abramowitz and I. A. Ryzhik, *Handbook of Mathematical Functions with Formulas, Graphs, and Mathematical Tables*, New York:Dover, 1972.

[16] "IWR6843, IWR6443 Single-Chip 60 to 64 GHz mmWave Sensor datasheet," 2022.